Electronic Supplementary Material (ESI) for Soft Matter.

Supplementary Material

Anionically modified N-(alkyl)acrylamide-based semi-IPN hybrid gels reinforced with SiO_2 for enhanced on-off switching and responsive properties

Birgul KALKAN and Nermin ORAKDOGEN

Istanbul Technical University, Department of Chemistry, Soft Materials Research Laboratory, 34469, Maslak, Istanbul, Turkey, Tel: +90-212-285-3305
*Corresponding author; e-mail: orakdogen@itu.edu.tr

ATR-FTIR spectra of semi-IPN hybrid gels

The spectrum of raw SiO_2 showed a broad band with a maximum at 3422 cm^{-1} indicated the water contribution (−OH). The peak at 3750 cm^{-1} was assigned to isolated silanols vibrations. The absorption peak at 1646 cm^{-1} was attributed to adsorbed water molecules deformation vibration, while C−H stretching vibration appeared at 2881 cm^{-1}. The discrete sharp band at 841 cm^{-1} was ascribed to O–H bending mode of hydrogen bonded, while Si-O in-plane stretching vibrations of silanol Si-OH groups were observed at 968 cm^{-1}. The symmetric mode of Si–O–Si band was detected at 785 cm^{-1}. The sharp band appearing at 1093-1059 cm^{-1} and the shoulder at around 1150 cm^{-1} were attributed to the transversal optical and longitudinal optical modes of Si-O-Si asymmetric stretching vibrations, respectively.

In ATR-FTIR spectra of semi-IPN P(NIPA-MA)/PAAm/SiP hybrid gels, the broad band between 3600 and 3000 cm^{-1} with a maximum at 3276 cm^{-1} contributed to N-H stretching vibrations and O-H stretching vibrations of carboxyl (COOH) groups from methacrylic acid, bound water in the structure and silanol (Si-OH) groups on the surface of the silica particles. The existence of intramolecular hydrogen bondings between C=O groups, N-H groups, and O-H groups on the silica surface results in a broad band between 3600 and 3000 cm^{-1}. Asymmetric deformation vibrations of C-H bond of methyl was detected at 1458 cm^{-1}, while the bands at 1386 and 1368 cm^{-1} were attributed to dimethyl symmetric deformation vibration (bending) of isopropyl group, $-CH(CH_3)_2$ of NIPA. C-N stretching (amide III) band at 1263 cm^{-1} in P(NIPA-MA)/PAAm spectrum is overlapped with Si-O-Si stretching band in the spectrum of hybrid samples. The peaks at 961 and 793 cm^{-1} are associated with Si-OH symmetric stretching and Si-O-Si bending vibrations, respectively. With the increase of SiO_2 content, the intensity of Si-O-Si stretching bands gradually increases in the hybrid samples, the intensities of peaks of functional groups associated with the network structure are weakened.

Table S1. Characteristic Functional Group Assignments

Characteristic Functional Group Assignments	Wavelength from literature (cm^{-1})	Peak Appearance Wavelength (cm^{-1})
N-H stretching	3300 [1], 3200 [2] 3428 - 3300 [3]	3285
Overtone of N-H bend		3076
C–H stretching	2974 (asym) [4] 2944 - 2641 [5] 2950 - 2870 [6] 2900 - 3000 [7]	2971 2936 2867
C=O stretching (amide I)	1649 [8], 1630 [9] 1650 [10]	1633
N-H bending (amide II)	1548 [a8], 1543 [10], 1544 [11]	1538
C–H bending	1456[8]	1458
C-H bending (isopropyl group)	1386 - 1367 [8] 1388 - 1368 [11]	1386-1368
Si-O-Si symmetric stretching	1091 [4,5], 1058 [9]	1056
Si-OH symmetric stretching	961 [4], 964 [5], 960 [9]	961
Si-O-Si bending	799 [4], 801 [5], 798 [9]	793

XRD results of semi-IPN hybrid gels

XRD patterns of neat SiO_2, silica-free semi-IPN P(NIPA-MA)/PAAm gel and semi-IPN hybrid P(NIPA-MA)/PAAm/SiP8-9 Hgel and Cgel samples containing 4.80 and 5.40% (w/v) of SiO_2, respectively, were investigated. In the diffractogram of neat SiO_2, the broad peak at $2\theta = 22.1°$ is the characteristic peak of amorphous silica particles. With addition of SiO_2, all samples showed an amorphous XRD halo. Silica-free semi-IPN P(NIPA-MA)/PAAm gel showed a sharp peak at $2\theta = 7.35°$ and a broad peak at $2\theta = 20.6°$ as an indication of a trend in the polymer chain to be organized. For semi-IPN hybrid Hgel and Cgel samples, the peak observed at $2\theta = 20.6°$ shifted to higher degree with the incorporation of silica into P(NIPA-MA)/PAAm structure, while the peak observed at 7.35° disappeared completely due to the high percentage of silica.

Temperature dependent swelling behavior of semi-IPN hybrid gels

Figure S1 shows the equilibrium volume swelling ratio φ_V of semi-IPN hybrid P(NIPA-MA)/PAAm/SiP Hgel and Cgel as a function of the external temperature and SiO_2 content. Photographs of P(NIPA-MA)/PAAm/SiP Hgels after swelling at 16 °C (left) and 70 °C (right) were presented.

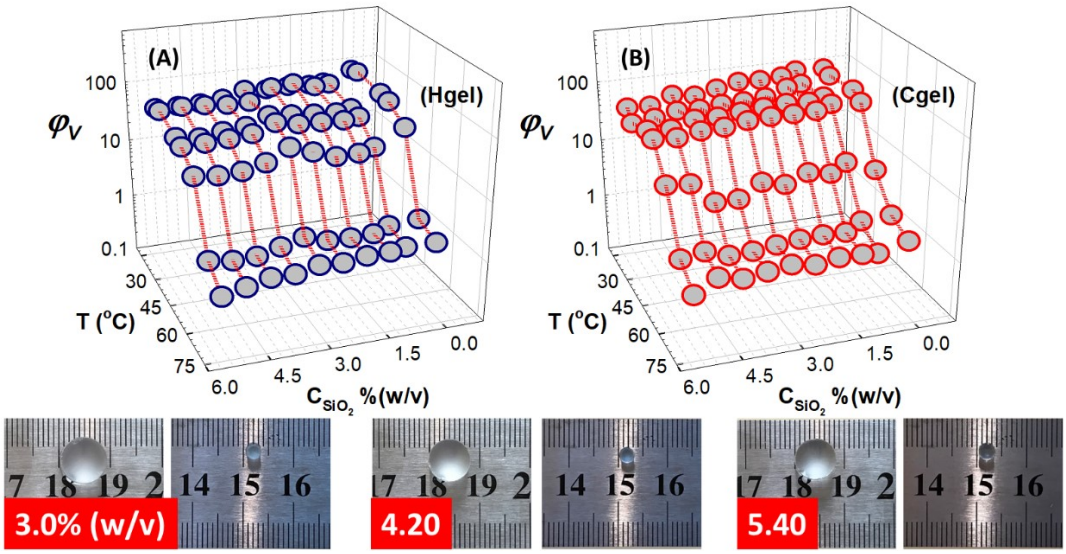

Figure S1. Equilibrium volume swelling ratio φ_V of semi-IPN hybrid P(NIPA-MA)/PAAm/SiP Hgel (A) and Cgel (B) shown as a function of the external temperature and SiO_2 content. Photographs of P(NIPA-MA)/PAAm/SiP Hgels after swelling at 16 °C (left) and 70 °C (right).

Salt-triggered swelling kinetics of semi-IPN hybrid gels

Figure S2 shows the plots of $\ln \varphi(t)/\varphi_W$ vs ln$t$ (A), water fraction $\varphi(t)/\varphi_W$ against $t^{1/2}$ (B) and $\ln(1-\varphi(t)/\varphi_W)$ vs t curves (C) of semi-IPN hybrid P(NIPA-MA)/PAAm/SiP Hgel obtained from the swelling in 10^{-5} M in aqueous NaCl solution. The values of the swelling exponents were obtained from the double logarithmic plot drawn between $\ln \varphi(t)/\varphi_W$ vs ln$t$ in Figure S2(A). From the slopes of the plot between $\varphi(t)/\varphi_W$ vs. $t^{1/2}$ given in Fig.S1(B), the values of early time diffusion coefficients D_E were calculated. As the silica content in the hybrid networks was increased, the diffusion coefficients decreased. For semi-IPN hybrid P(NIPA-MA)/PAAm/SiP Hgel ranged from 1.454×10^{-7} to 3.809×10^{-7} cm^2 s^{-1}. By the late-time approximation, the slope of $\ln(1-\varphi(t)/\varphi_W)$ vs t curves of semi-IPN hybrid gels in Fig. S2(C) obtained from the swelling in 10^{-5} M in aqueous NaCl solution was used to determine the late-time diffusion coefficients, D_L. The early-time diffusion coefficients were lower than the late-time values due to the greater extent of the swelling in longer swelling times.

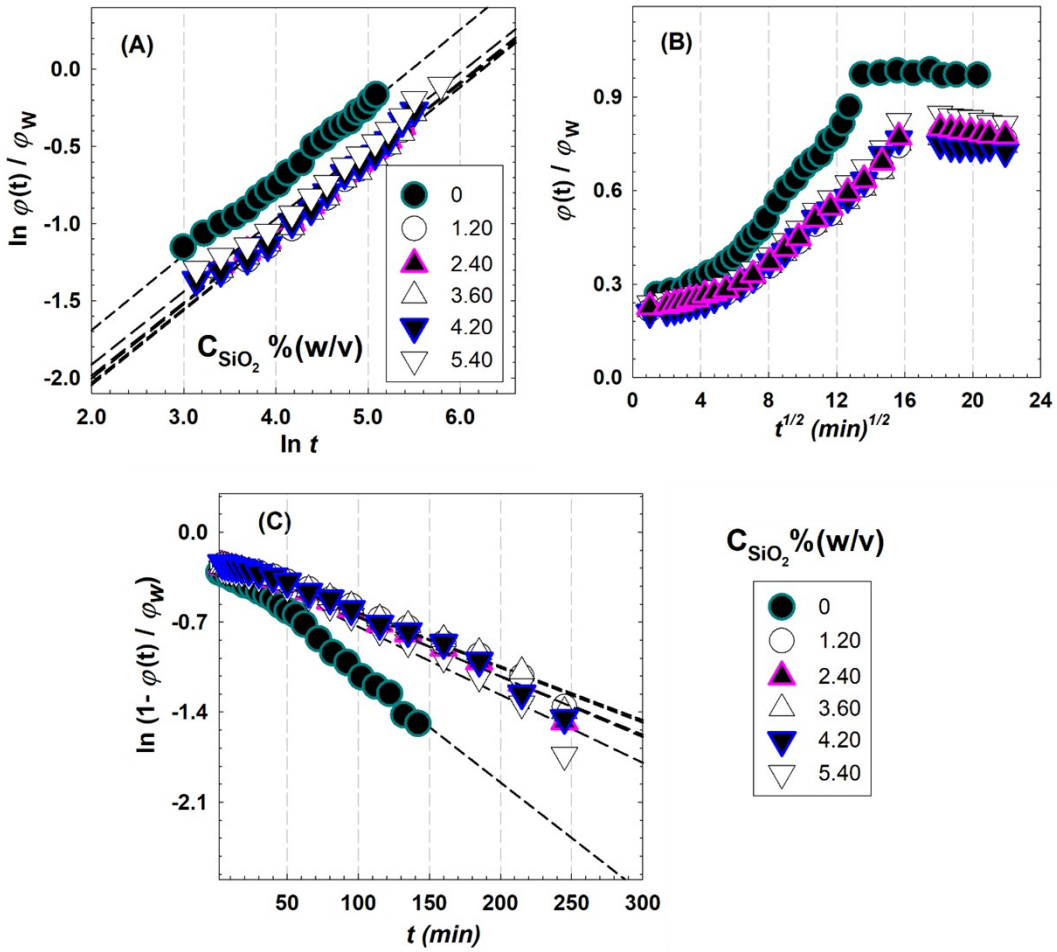

Figure S2. (A) $\ln \varphi(t)/\varphi_W$ vs ln$t$, (B) water fraction $\varphi(t)/\varphi_W$ against $t^{1/2}$ and (C) $\ln(1-\varphi(t)/\varphi_W)$ vs t curves of semi-IPN hybrid P(NIPA-MA)/PAAm/SiP Hgel obtained from the swelling in 10^{-5} M in aqueous NaCl solution.

Adsorbent characteristics of semi-IPN hybrid gels

The adsorption performance of the semi-IPN hybrids was tested for MV dye concentration 5 and 10 mg/L. Figure S3 shows the results for adsorption of MV dye by semi-IPN hybrid P(NIPA-MA)/PAAm/SiP gels prepared at different SiO_2 content as a function of contact time.

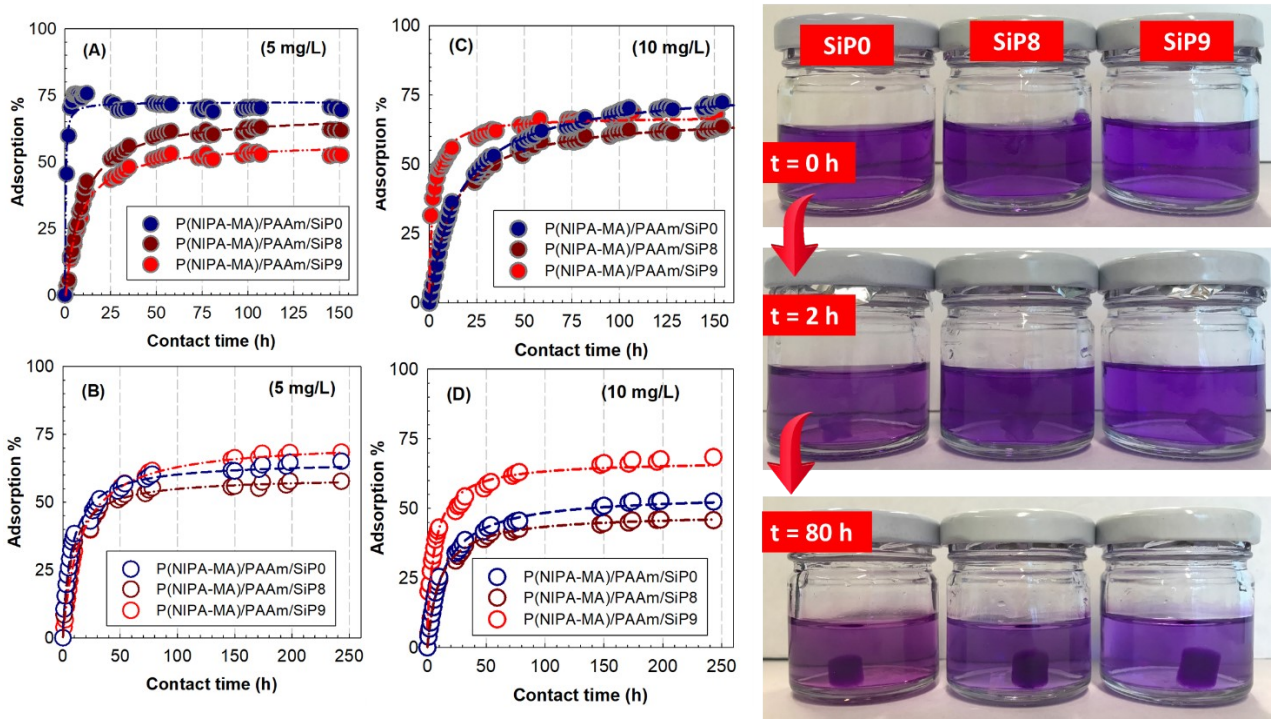

Figure S3. Adsorption of MV dye by semi-IPN hybrid P(NIPA-MA)/PAAm/SiP Hgel (A, C) and Cgel (B, D) prepared at different SiO_2 content as a function of contact time. MV dye concentration: 5 (left plots) and 10 mg/L (right plots).

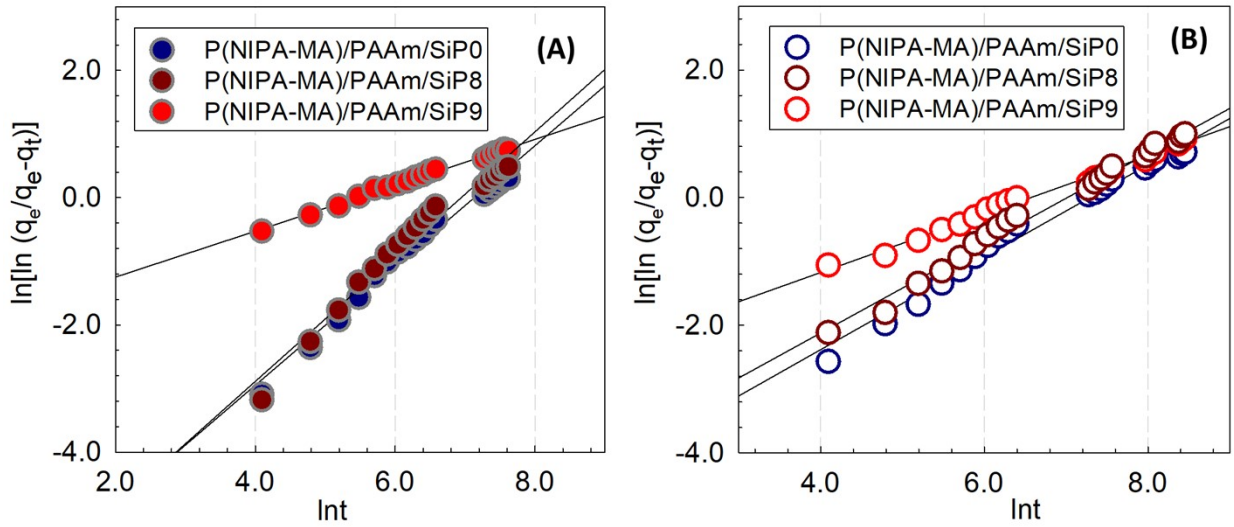

Figure S4. Dye adsorption kinetics fitted with Avrami kinetic model (A, B) for semi-IPN hybrid P(NIPA-MA)/PAAm/SiP Hgel (left) and Cgel (right). The solid line indicates the model-fit in the experimental data. MV concentration: 10 mg/L.

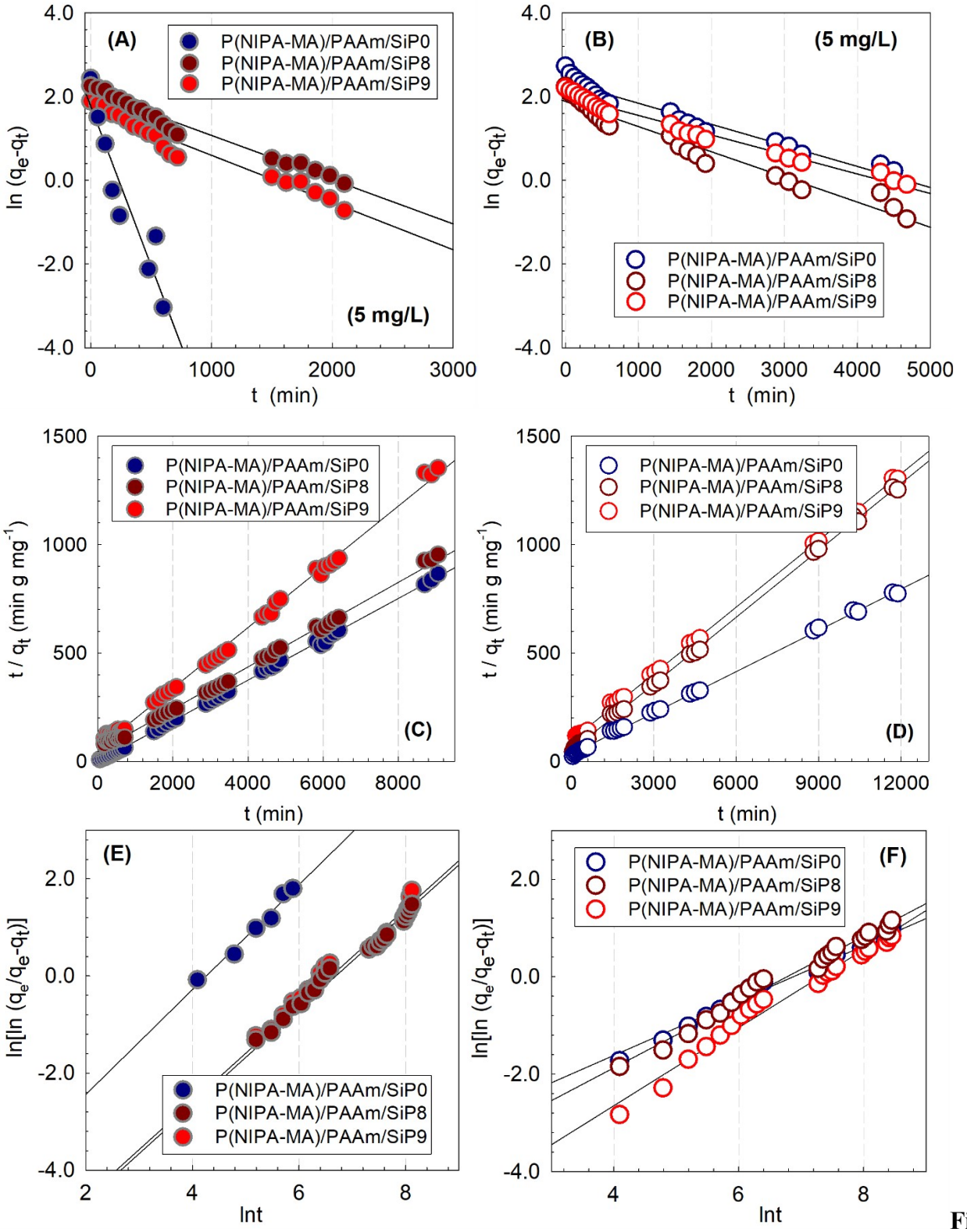

Figure S5. Dye adsorption kinetics fitted with Lagergren pseudo-first order kinetic model (A, B), Ho second order kinetic model (C, D), and Avrami kinetic model (E, F) for semi-IPN hybrid

P(NIPA-MA)/PAAm/SiP Hgel (left) and Cgel (right). The solid line indicates the model-fit in the experimental data. MV concentration: 5 mg/L.

Figure S5-S7 are the results of adsorption kinetics models toward the experiments. Figure S5 presents dye adsorption kinetics fitted with Lagergren pseudo-first order kinetic model (A,B), Ho second order kinetic model (C,D), and Avrami kinetic model (E,F) for semi-IPN hybrid P(NIPA-MA)/PAAm/SiP Hgel (left) and Cgel (right) in initial MV concentration of 5 mg/L. The results for dye adsorption kinetics fitted with Elovich kinetic model (A,B), and fractional power kinetic model (C,D) are presented in Figure S6 and S7 in initial MV concentration of 5 mg/L and 10 mg/L, respectively. Kinetic parameters of pseudo-first-order, pseudo-second-order, Avrami, Elovich, fractional power and intraparticle diffusion models for total MV sorption onto semi-IPN P(NIPA-MA)/PAAm/SiP Cgels for initial MV concentration 5 mg L^{-1} are presented in Table S2. Thermodynamic parameters for adsorption of MV dye and adsorption capacity of P(NIPA-MA)/PAAm/SiP Cgel calculated from various kinetic models are shown in Table S3.

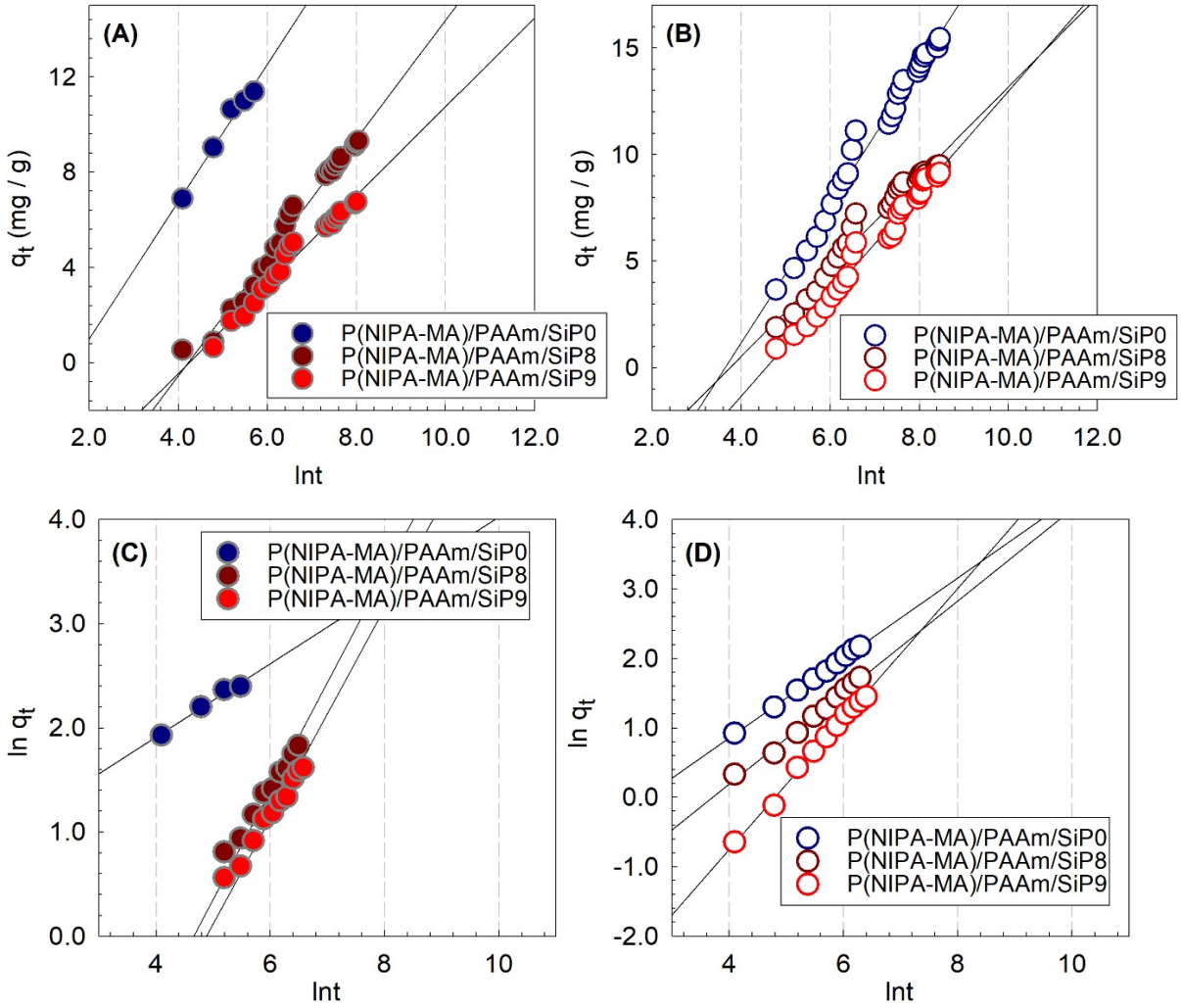

Figure S6. Dye adsorption kinetics fitted with Elovich kinetic model (A,B), and fractional power kinetic model (C,D) for semi-IPN hybrid P(NIPA-MA)/PAAm/SiP Hgel (left) and Cgel (right). The solid line indicates the model-fit in the experimental data. MV concentration: 5 mg/L

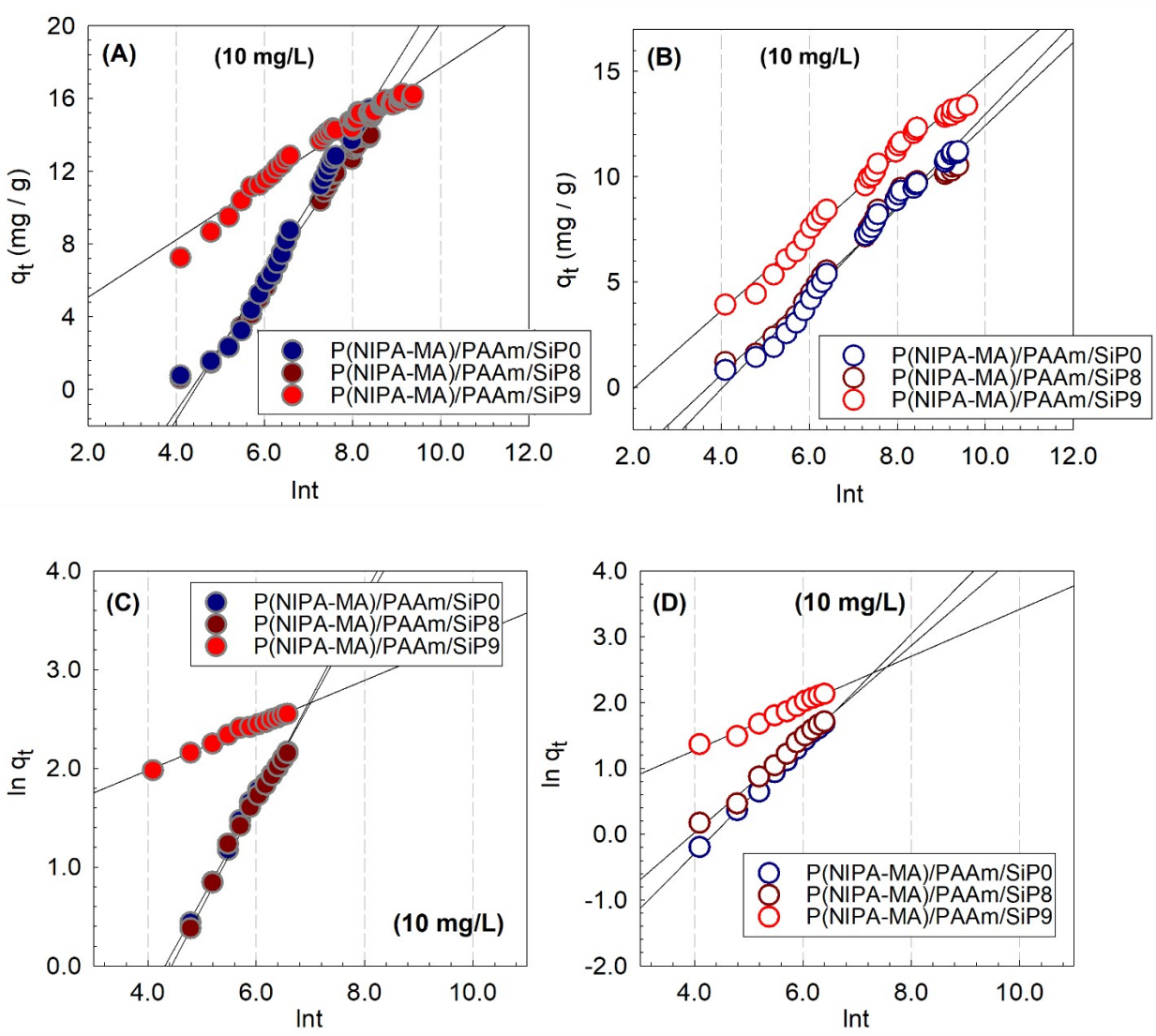

Figure S7. Dye adsorption kinetics fitted with Elovich kinetic model (A,B), and fractional power kinetic model (C,D) for semi-IPN hybrid P(NIPA-MA)/PAAm/SiP Hgel (left) and Cgel (right). The solid line indicates the model-fit in the experimental data. MV concentration: 10 mg/L

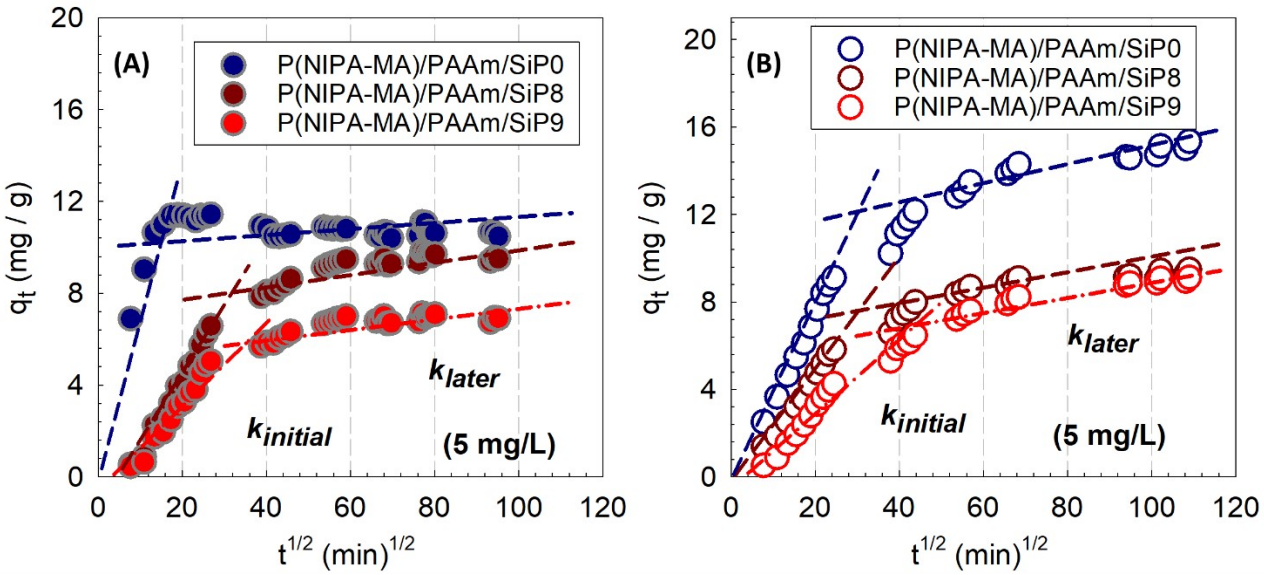

Figure S8. Dye adsorption mechanism fitted with intraparticle diffusion model for semi-IPN hybrid P(NIPA-MA)/PAAm/SiP Hgel (A) and Cgel (B). The solid line indicates the model-fit in the experimental data. MV concentration: 5 mg/L.

Table S2. Kinetic parameters of pseudo-first-order, pseudo-second-order, Avrami, Elovich, fractional power and intraparticle diffusion models for total MV sorption onto semi-IPN P(NIPA-MA)/PAAm/SiP Cgels. Initial MV concentration: 5 mg L^{-1}

Pseudo-first order model			Elovich model		
Sample	$k_1 \times 10^{-3}$ (min^{-1})	R^2	α (mg/g min)	β (g/mg)	R^2
P(NIPA-MA)/PAAm/SiP0	0.502	0.9485	0.084	0.307	0.9838
P(NIPA-MA)/PAAm/SiP8	0.601	0.9562	0.049	0.474	0.9680
P(NIPA-MA)/PAAm/SiP9	0.466	0.9769	0.024	0.419	0.9815

Pseudo-second order model			Weber-Morris model			
Sample	$k_2 \times 10^{-3}$ (min^{-1})	R^2	$k_{initial}$ (mg g^{-1} $min^{-1/2}$)	R^2	k_{later} (mg g^{-1} $min^{-1/2}$)	R^2
P(NIPA-MA)/PAAm/SiP0	0.122	0.9991	0.408	0.9971	0.041	0.8888
P(NIPA-MA)/PAAm/SiP8	0.220	0.9994	0.282	0.9875	0.018	0.8107
P(NIPA-MA)/PAAm/SiP9	0.109	0.9996	0.163	0.9506	0.034	0.8861

Fractional power model				Avrami model		
Sample	ν_{fr} (min^{-1})	$k_{fr} \times 10^{-2}$ (mg /g)	R^2	n_{Av}	$k_{Av} \times 10^{-3}$ (min^{-1})	R^2
P(NIPA-MA)/PAAm/SiP0	0.576	8.041	0.9989	0.561	0.103	0.9858
P(NIPA-MA)/PAAm/SiP8	0.659	2.439	0.9906	0.674	0.114	0.9336
P(NIPA-MA)/PAAm/SiP9	0.939	0.821	0.9951	0.800	0.067	0.9673

Table S3. Thermodynamic parameters for adsorption of MV dye and adsorption capacity of P(NIPA-MA)/PAAm/SiP Cgel calculated from various kinetic models. Initial MV concentration: 5 mg L^{-1}.

Sample	Exp. q_e (mg/g)	Pseudo-first order $q_{e,calc}$ (mg/g)	Pseudo-second order $q_{e,calc}$ (mg/g)	ΔG^o (kJ/mol K)
P(NIPA-MA)/PAAm/SiP0	11.150	8.544	11.901	-2.163
P(NIPA-MA)/PAAm/SiP8	10.488	7.897	11.005	-1.686
P(NIPA-MA)/PAAm/SiP9	13.390	7.909	13.584	-3.633

Stress-strain isotherms of semi-IPN hybrid gels

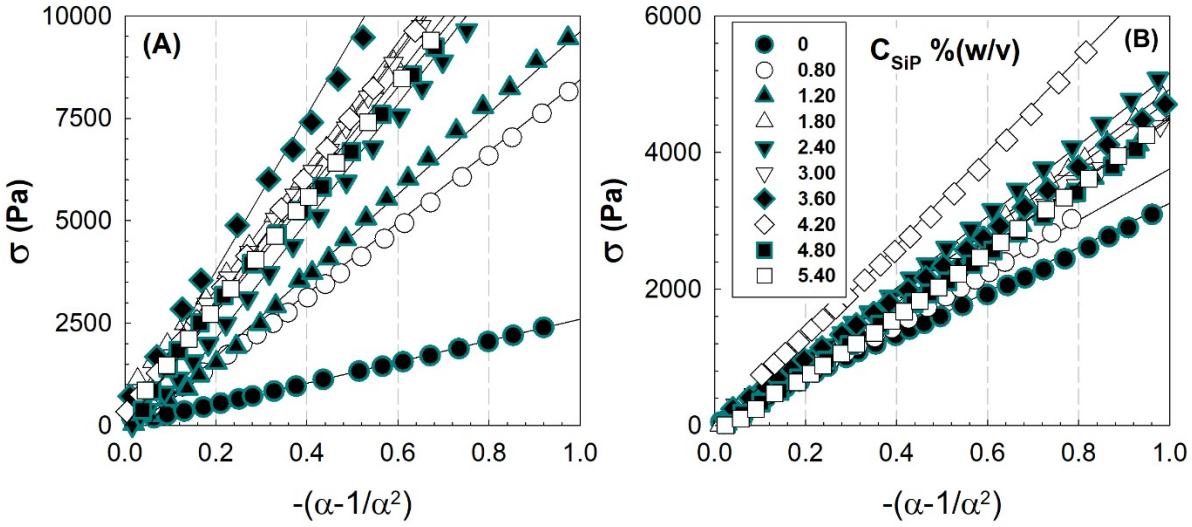

Figure S9. Stress-strain isotherms of semi-IPN hybrid P(NIPA-MA)/PAAm/SiP Cgel (A) and Hgel (B) measured after equilibrium swelling in water.

References

[1] Hebeish, A., Farag, S., Sharaf, S., & Shaheen, T. I. (2014). Thermal responsive hydrogels based on semi interpenetrating network of poly (NIPAm) and cellulose nanowhiskers. Carbohydrate polymers, 102, 159-166.

[2] Seddiki, N., & Aliouche, D. (2013). Synthesis, rheological behavior and swelling properties of copolymer hydrogels based on poly (N-isopropylacrylamide) with hydrophilic monomers. Bulletin of the Chemical Society of Ethiopia, 27(3), 447-457.

[3] Wei, J., Chen, Y., Liu, H., Du, C., Yu, H., & Zhou, Z. (2016). Thermo-responsive and compression properties of TEMPO-oxidized cellulose nanofiber-modified PNIPAm hydrogels. Carbohydrate polymers, 147, 201-207.

[4] Su, M., Liu, Y., Zhang, Y., Wang, Z., Li, Y., & He, P. (2018). Robust and underwater superoleophobic coating with excellent corrosion and biofouling resistance in harsh environments. Applied Surface Science, 436, 152-161.

[5] Mittal, H., Maity, A., & Ray, S. S. (2015). Synthesis of co-polymer-grafted gum karaya and silica hybrid organic–inorganic hydrogel nanocomposite for the highly effective removal of methylene blue. Chemical Engineering Journal, 279, 166-179.

[6] Agorku, E. S., Mittal, H., Mamba, B. B., Pandey, A. C., & Mishra, A. K. (2014). Fabrication of photocatalyst based on Eu3+-doped ZnS–SiO2 and sodium alginate core shell nanocomposite. International journal of biological macromolecules, 70, 143-149.

[7] Sun, L., Zhang, X., Zheng, C., Wu, Z., & Li, C. (2013). A pH Gated, Glucose-Sensitive Nanoparticle Based on Worm-Like Mesoporous Silica for Controlled Insulin Release. The Journal of Physical Chemistry B, 117(14), 3852–3860.

[8] Kang, X., Cheng, Z., Yang, D., Ma, P. A., Shang, M., Peng, C., ... & Lin, J. (2012). Design and synthesis of multifunctional drug carriers based on luminescent rattle-type mesoporous silica microspheres with a thermosensitive hydrogel as a controlled switch. Advanced Functional Materials, 22(7), 1470-1481.
[9] Zhang, X., Wu, B., Sun, S., & Wu, P. (2020). Hybrid Materials from Ultrahigh-Inorganic-Content Mineral Plastic Hydrogels: Arbitrarily Shapeable, Strong, and Tough. Advanced functional materials, 30(19), 1910425.
[10] Wei, J., Chen, Y., Liu, H., Du, C., Yu, H., & Zhou, Z. (2016). Thermo-responsive and compression properties of TEMPO-oxidized cellulose nanofiber-modified PNIPAm hydrogels. Carbohydrate polymers, 147, 201-207.
[11] Li, G., Yu, N., Gao, Y., Tao, Q., & Liu, X. (2016). Polymeric hollow spheres assembled from ALG-g-PNIPAM and β-cyclodextrin for controlled drug release. International journal of biological macromolecules, 82, 381-386.